Theory of transient stimulated Raman scattering in H_2

Burke Ritchie*
Sandia National Laboratories, Albuquerque, New Mexico 87185
(Received 3 November 1986)

Calculations are performed for stimulated Raman scattering in H_2 in the transient regime. The production of anti-Stokes radiation depends strongly on phase matching in the dispersive medium, and a predictive theory requires at least two spatial dimensions to describe the process.

I. INTRODUCTION

The classical theory of stimulated Raman scattering (SRS) has been available in both the steady-state[1,2] and the transient[3,4] regimes for quite awhile. Recently, the observation[5,7] of the efficient production of anti-Stokes (A) radiation in H_2 has led to a renewed interest in the theory of higher-order SRS. Very recently a theory[8] has appeared describing the generation of anti-Stokes radiation to eighth order. This is a transient theory which includes depletion of the ground state of the molecular target; however, an important effect, phase mismatch among the various light waves due to their dispersion in the medium, is ignored. In the present paper we ignore ground-state depletion (which is negligible in H_2 for GW cm^{-2} laser irradiation for pulsewidths less than 1 ns) but include phase mismatch. The latter is known to be profoundly important[1] in steady state and is found to be so here for transient scattering of pulses having widths less than 200 ps. In fact, all anti-Stokes generation is suppressed for collinear laser (L), Stokes (S), and anti-Stokes waves. The origin of this suppression is the rapid oscillation with propagation distance of terms which couple the anti-Stokes to the Stokes waves. The first Stokes wave is "seeded" (i.e., is assumed to have an initial input intensity) as the source of SRS (ignoring spontaneous Raman scattering or "noise" as a source); thus, the Stokes—anti-Stokes coupling is the source of anti-Stokes generation, and the first-order term oscillates with distance along a collinear path with frequency mismatch $\Delta k = 2k_L - k_S - k_A$ cm^{-1} ($k_j = n_j\omega_j/c$, where n_j is the jth wave index of refraction and ω_j is the radian frequency), which for H_2 (based on accurate theoretical calculations[9]) is about $1P$ cm^{-1} (where P is the gas pressure in atm) for ω_L, $\omega_S = \omega_L - \Delta\omega$, and $\omega_A = \omega_L + \Delta\omega$ corresponding to 51 719-cm radiation (ArF eximer laser) and a 0-1 vibrational level separation $\Delta\omega$ of 4158.55 cm^{-1}.

In a noncollinear calculation the angles of the Stokes and anti-Stokes waves relative to the direction of the laser wave can be adjusted[10] so that $\Delta k \simeq 0$ (corresponding to the assumption[8] of $\Delta k = 0$ in a collinear calculation). However, additional terms depending on the degrees of freedom transverse to the propagation direction of the laser (forward direction) are generated in the wave equations, the most important of which are the transverse derivatives of the Stokes and anti-Stokes pulse envelopes. Calculations are performed with and without the transverse derivatives, and it is found that the accurate prediction of Stokes and anti-Stokes conversion efficiencies depends strongly on the correct description of these terms.

II. THEORY

The Maxwell-Bloch theory in the form presented by Icsevgi and Lamb[11] (IL) is extended to Raman scattering. The IL theory was originally formulated for an input laser pulse incident on an inverted population of two-level atoms, and it contains a detailed prescription for coupling Maxwell's equation for the laser to the Heisenberg equation for the atomic density matrix $\dot{\rho} = (i\hbar)^{-1}[H,\rho]$, where ρ is the density operator and H is the Hamiltonian for the atomic target and classical radiation field. Application to Raman scattering requires that the quantum states used to represent ρ and to average the macroscopic dipole moment in Maxwell's equation be perturbed to first order in a potential of the form

$$V = \tfrac{1}{2}\left[\mathcal{E}_j e^{i(\mathbf{k}_j\cdot\mathbf{r}-\omega_j t)} + \mathcal{E}_j^* e^{-i(\mathbf{k}_j\cdot\mathbf{r}-\omega_j t)}\right]\cdot e\mathbf{r} ,$$

where $\mathcal{E}_j$, $\mathbf{k}_j$, and ω_j are the jth electromagnetic pulse envelope, propagation vector, and frequency, and $\mathbf{r}$ is an electron position. The effect of the perturbation by a pump field of ω_L is to cause the spectrum of the electromagnetic field to have two additional components at $\omega_L \pm \Delta\omega$ (where $\Delta\omega$ is the frequency of an internal transition in the target atom or molecule). If this process is generalized to include the first-order perturbation of the target by the two additional pulses, then two more frequency components at $\omega_L \pm 2\Delta\omega$ are introduced into the spectrum, and so on. Thus the frequency spectrum of the electromagnetic field will consist of a central component at ω_L and the nth-order Stokes, and anti-Stokes components at $\omega_L - n\Delta\omega$, $\omega_L + n\Delta\omega$, respectively.

The electric field strength is expanded,

$$E = \tfrac{1}{2}\left\{\mathcal{E}_L(z,t)e^{i(k_L z-\omega_L t)} + \sum_{j=1}^{n}\left[\mathcal{E}_{S_j}(\mathbf{r},t)e^{i(\mathbf{k}_{S_j}\cdot\mathbf{r}-\omega_{S_j}t)} + \mathcal{E}_{A_j}(\mathbf{r},t)e^{i(\mathbf{k}_{A_j}\cdot\mathbf{r}-\omega_{A_j}t)}\right]\right\} + \text{c.c.} , \quad (1)$$

where the summation runs over Stokes and anti-Stokes

waves of order 1 to n. The linear polarization directions of all waves in Eq. (1) are assumed to be along y and $\mathbf{k}_L$ and $\mathbf{k}_{A_j}$ are assumed to be along z or nearly along z. Figure 1 gives a vector diagram[1] which illustrates the phase-matching condition for the first-order Stokes and anti-Stokes wave vectors,

$$\Delta k_z = 2k_L - k_{S_1}\cos\theta_{S_1} - k_{A_1}\cos\theta_{A_1} , \tag{2a}$$

$$\Delta k_x = -k_{S_1}\sin\theta_{S_1} + k_{A_1}\sin\theta_{A_1} , \tag{2b}$$

$$\Delta k_y = 0 , \tag{2c}$$

where the angles are assumed to be small. The calculations are therefore performed in the xz plane, and the pulse envelopes are functions of z and t for the laser and x, z, and t for the Stokes and anti-Stokes waves. The effect of small nonzero values in the angles on Δk_z is large due to the large magnitudes of the individual $\mathbf{k}$ vectors.

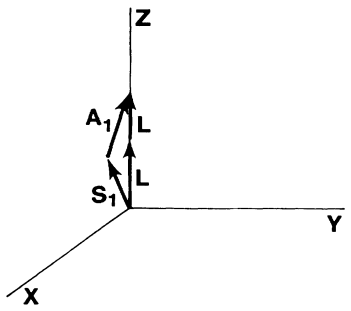

FIG. 1. Vector diagram. See text for definitions.

The equations for the slowly varying pulse envelopes are derived according to the prescriptions of IL,[11]

$$\frac{\partial \mathcal{E}_L(z,t)}{\partial z} + \frac{1}{v_L}\frac{\partial \mathcal{E}_L}{\partial t}(z,t) = \frac{2\pi i\omega_L}{n_L c}\left[p_{S_1}\mathcal{E}_{S_1}(x,z,t)\rho_{ge}^{(S_1)} + p_{A_1}\mathcal{E}_{A_1}(x,z,t)\rho_{eg}^{(A_1)}\right] , \tag{3a}$$

$$\theta_{S_j}\frac{\partial}{\partial x}\mathcal{E}_{S_j}(x,z,t) + \frac{\partial}{\partial z}\mathcal{E}_{S_j}(x,z,t) + \frac{1}{v_{S_j}}\frac{\partial \mathcal{E}_{S_j}}{\partial t}(x,z,t) = \frac{2\pi i\omega_{S_j}}{n_{S_j}c}\left[p_{S_j}\mathcal{E}_{S_{j-1}}(x,z,t)\rho_{eg}^{(S_j)} + p_{S_{j+1}}\mathcal{E}_{S_{j+1}}(x,z,t)\rho_{ge}^{(S_j+1)}\right] , \tag{3b}$$

$$-\theta_{A_j}\frac{\partial}{\partial x}\mathcal{E}^*_{A_j}(x,z,t) + \frac{\partial}{\partial z}\mathcal{E}^*_{A_j}(x,z,t) + \frac{1}{v_{A_j}}\frac{\partial \mathcal{E}^*_{A_j}}{\partial t}(x,z,t) = -\frac{2\pi i\omega_{A_j}}{n_{A_j}c}\left[p_{A_j}\mathcal{E}^*_{A_{j-1}}(x,z,t)\rho_{eg}^{(A_j)} + p_{A_{j+1}}\mathcal{E}^*_{A_{j+1}}(x,z,t)\rho_{ge}^{(A_j+1)}\right] , \tag{3c}$$

where for Eqs. (3b) and (3c) $j \geq 1$ and $\mathcal{E}_{S_0} = \mathcal{E}_{A_0} = \mathcal{E}_L$, $\omega_{S_0} = \omega_{A_0} = \omega_L$, and $n_{S_0} = n_{A_0} = n_L$. In a first-order ($j = 1$) calculation[1] the second terms in Eqs. (3b) and (3c) are dropped. The coherent element of the molecular density matrix is $\rho_{ge} = a_g^* a_e N_0$ and $\rho_{eg} = \rho_{ge}^*$, where a_g, a_e are the time-dependent amplitudes of the ground, first excited vibrational states of H_2, and N_0 is the gas-atom number density. The elements in Eqs. (3) are the slowly varying parts of ρ_{ge},

$$\rho_{ge}^{(S_j)} = \rho_{ge}e^{-i\delta_{S_j}t} , \tag{4a}$$

$$\rho_{ge}^{(A_j)} = \rho_{ge}e^{-i\delta_{A_j}t} , \tag{4b}$$

$$\delta_{S_j} = \omega_e - \omega_g - \omega_{S_{j-1}} + \omega_{S_j} , \tag{4c}$$

$$\delta_{A_j} = \omega_e - \omega_g + \omega_{A_{j-1}} - \omega_{A_j} . \tag{4d}$$

The p parameters in Eqs. (3) in cm^3 are defined

$$p_{S_j} = \langle F_e(R) \,|\, \alpha_0(\omega_{S_{j-1}}, R) \,|\, F_g(R)\rangle , \tag{5a}$$

$$p_{A_j} = \langle F_e(R) \,|\, \alpha_0(\omega_{A_j}, R) \,|\, F_g(R)\rangle , \tag{5b}$$

where $\alpha_0(\omega R) = \frac{1}{3}[\alpha_{||}(\omega_a, R) + 2\alpha_\perp(\omega_a, R)]$ is the isotropic part of frequency-dependent polarizability[9] of H_2 as a function of internuclear distance R, and F_g, F_e are the ground, and first-excited vibrational (i.e., nuclear radial) wave functions. The p parameters [and $\alpha_0(\omega_a, R)$ averaged using $F_g(R)$, needed to evaluate the indexes of refraction $n_{S_{j-1}}$ and $n_{A_{j-1}}$] are taken directly from Ref. 9. In the x derivatives in Eqs. (3), $\sin\theta_a \simeq \theta_a$. The right-hand sides (rhs) of Eqs. (3) follow from a thermal average over the rotational (J) distribution of the molecular gas; hence, this result depends only on the isotropic part of the p parameters. It is not correct, however, to assume that ρ_{ge} does not vary with the molecular J level since there is a loss of laser-induced coherence due to intermolecular collisions[12] in the gas. In order to simplify the calculation we assume only the $J = 1$ level is populated (pure ortho-H_2). (At room temperature about 66% of the molecules are in the $J = 1$ level.) Since the pulsewidth at half maximum in the present calculations is only about 15% of a relaxation time characteristic of J collisions[12] at 10-atm gas pressure (i.e., the medium polarization is nearly coherent), the present results should not differ appreciably from those of experiments on a room-temperature gas. The Doppler average of the rhs of Eqs. (3) is unnecessary

since Doppler broadening is much smaller than collisional broadening at the gas pressures considered here. Finally, the transverse Laplacian is negligible in these studies since the characteristic diffraction length of any of the waves, $l=kw^2$, is large such that $\theta_{s_1}\simeq\theta_{A_1}\gg\theta_d$, where θ_d is the divergence angle due to diffraction.

Neglecting ground-state population depletion, the density-matrix elements are defined by the equations

$$\frac{\partial\rho_{ge}^{(S_j)}}{\partial t}=(-i\delta_{S_j}-\gamma_{c/2})\rho_{ge}^{(S_j)}+\frac{N_0 i}{4\hbar}\sum_{j'=1}^{n}(p_{S_{j'}}\mathcal{E}_{S_{j'-1}}\mathcal{E}_{S_{j'}}^{*}e^{-i(\Delta\mathbf{k}_{S_jS_{j'}}\cdot\mathbf{r}-\Delta\delta_{S_jS_{j'}}t)}+p_{A_{j'}}\mathcal{E}_{A_{j'-1}}^{*}\mathcal{E}_{A_{j'}}e^{-i(\Delta\mathbf{k}_{S_jA_{j'}}\cdot\mathbf{r}-\Delta\delta_{S_jA_{j'}}t)}), \tag{6a}$$

$$\frac{\partial\rho_{ge}^{(A_j)}}{\partial t}=(-i\delta_{A_j}-\gamma_{c/2})\rho_{ge}^{(A_j)}+\frac{N_0 i}{4\hbar}\sum_{j'=1}^{n}(p_{S_{j'}}\mathcal{E}_{S_{j'-1}}\mathcal{E}_{S_{j'}}^{*}e^{i(\Delta\mathbf{k}_{A_jS_{j'}}\cdot\mathbf{r}-\Delta\delta_{A_jS_{j'}}t)}+p_{A_{j'}}\mathcal{E}_{A_{j'-1}}^{*}\mathcal{E}_{A_{j'}}e^{-i(\Delta\mathbf{k}_{A_jA_{j'}}\cdot\mathbf{r}-\Delta\delta_{A_jA_{j'}}t)}), \tag{6b}$$

$$\Delta\mathbf{k}_{S_jS_{j'}}=\mathbf{k}_{S_{j-1}}-\mathbf{k}_{S_j}-\mathbf{k}_{S_{j'-1}}+\mathbf{k}_{S_{j'}}, \tag{6c}$$

$$\Delta\mathbf{k}_{S_jA_{j'}}=\mathbf{k}_{S_{j-1}}-\mathbf{k}_{S_j}+\mathbf{k}_{A_{j'-1}}-\mathbf{k}_{A_{j'}}, \tag{6d}$$

$$\Delta\mathbf{k}_{A_jS_{j'}}=\mathbf{k}_{A_{j-1}}-\mathbf{k}_{A_j}+\mathbf{k}_{S_{j'-1}}-\mathbf{k}_{S_{j'}}, \tag{6e}$$

$$\Delta\mathbf{k}_{A_jA_{j'}}=\mathbf{k}_{A_{j-1}}-\mathbf{k}_{A_j}-\mathbf{k}_{A_{j'-1}}+\mathbf{k}_{A_{j'}}, \tag{6f}$$

where the $\Delta\delta$ parameters [which, along with Eqs. (4c) and (4d), are zero in the calculations] can be derived from the $\Delta\mathbf{k}$ parameters by setting the indexes of refraction in the latter equal to zero. The parameter γ_c is the collisional rate of decay of the coherence induced by the laser in $J=1$ molecules. It is taken from recent experimental measurements[12] [$\gamma_c=2\pi\Delta\nu\,(0.9122)P$, where $\Delta\nu$ is[12] 0.0524 GHz/amagat and P is the gas pressure in atm for 0.9122 amagat/atm]. Any loss of coherence due to laser-pulse phase or amplitude fluctuations is ignored as small compared to γ_c.

Despite their complicated appearance, Eqs. (3)–(6) are easy to interpret. In Eq. (3a) the first and second terms contain terms which produce loss and growth in the laser, matching the growth and loss in the first-order Stokes and anti-Stokes waves, respectively. The first terms in Eqs. (3b) and (3c) for $j=1$ contain terms which produce the growth and loss in the Stokes and anti-Stokes waves matching the loss and growth in the laser, respectively. For $j>1$ the first and second terms in Eq. (3b) contain terms which produce growth and loss in the jth Stoke wave due to loss and growth in the $(j-1)$th Stokes and $(j+1)$th Stokes waves, respectively. For $j>1$ the first and second terms in Eq. (3c) contain terms which produce loss and growth in the jth anti-Stokes wave due to growth and loss in the $(j-1)$th and $(j+1)$th anti-Stokes waves, respectively. In other words, laser is converted to first-order Stokes, which is then converted to second-order Stokes, etc., and first-order anti-Stokes is converted to laser, second-order anti-Stokes is converted to first-order anti-Stokes, etc. The origin of the anti-Stokes waves is through the coupling to the Stokes waves, and this is more easily seen from the set of first-order equations given explicitly below.

Since the equations for ω_L, ω_{s_1}, and ω_{A_1} reduce in the steady-state limit to the equations of Bloembergen-Shen (BS),[1] it is instructive to list them separately. Having eliminated the density-matrix elements by solving Eqs. (6a)–(6b) and substituting the result into Eqs. (3), these are

$$\theta_{S_1}\frac{\partial\mathcal{E}_{S_1}(\tau)}{\partial x}+\frac{\partial\mathcal{E}_{S_1}(\tau)}{\partial z}=\frac{N_0\pi\omega_{S_1}}{2\hbar c}e^{i(\delta_{S_1}+i\gamma_c/2)\tau}\mathcal{E}_L(\tau)\left[p_{S_1}^2\int_0^\tau d\tau' e^{-i(\delta_{S_1}+i\gamma_c/2)\tau'}\mathcal{E}_L^{*}(\tau')\mathcal{E}_{S_1}(\tau')\right.$$
$$\left.+p_{S_1}p_{A_1}e^{i[\Delta k_z-(\Delta\delta/c)]z}e^{i\Delta k_x x}\times\int_0^\tau d\tau' e^{-i(\delta_{A_1}+i\gamma_{c/2})\tau'}\mathcal{E}_L(\tau')\mathcal{E}_{A_1}^{*}(\tau')\right], \tag{7a}$$

$$-\theta_{A_1}\frac{\partial\mathcal{E}_{A_1}^{*}(\tau)}{\partial x}+\frac{\partial\mathcal{E}_{A_1}^{*}(\tau)}{\partial z}=\frac{-N_0\pi\omega_{A_1}}{2\hbar c}e^{i(\delta_{A_1}+i\gamma_c/2)\tau}\mathcal{E}_L^{*}(\tau)$$
$$\times\left[p_{A_1}p_{S_1}e^{-i[\Delta k_z-(\Delta\delta/c)]z}e^{-i\Delta k_x x}\int_0^\tau d\tau' e^{-i(\delta_{S_1}+i\gamma_c/2)\tau'}\mathcal{E}_L^{*}(\tau')\mathcal{E}_{S_1}(\tau')\right.$$
$$\left.+p_{A_1}^2\int_0^\tau d\tau' e^{-i(\delta_{A_1}+i\gamma_c/2)\tau'}\mathcal{E}_L(\tau')\mathcal{E}_{A_1}^{*}(\tau')\right], \tag{7b}$$

$$\frac{\partial \mathcal{E}_L(\tau)}{\partial z} = -\frac{N_0 \pi \omega_L}{2\hbar c} e^{-i(\delta_{S_1} - i\gamma_c/2)\tau} \mathcal{E}_{S_1}(\tau) \left[p_{S_1}^2 \int_0^\tau d\tau' e^{i(\delta_{S_1} - i\gamma_c/2)\tau'} \mathcal{E}_{S_1}^*(\tau') \mathcal{E}_L(\tau') + p_{S_1} p_{A_1} e^{-i[\Delta k_z - (\Delta\delta/c)]z} e^{-i\Delta k_x x} \times \int_0^\tau d\tau' e^{i(\delta_{A_1} - i\gamma_c/2)\tau'} \mathcal{E}_{A_1}(\tau') \mathcal{E}_L^*(\tau') \right] \tag{7c}$$

$$+ \frac{N_0 \pi \omega_L}{2\hbar c} e^{i(\delta_{A_1} + i\gamma_c/2)\tau} \mathcal{E}_{A_1}(\tau) \left[p_{A_1}^2 \int_0^\tau d\tau' e^{-i(\delta_{A_1} + i\gamma_c/2)\tau'} \mathcal{E}_{A_1}^*(\tau') \mathcal{E}_L(\tau') + p_{A_1} p_{S_1} e^{-i[\Delta k_z - (\Delta\delta/c)]z} e^{-i\Delta k_x x} \int_0^\tau d\tau' e^{-i(\delta_{S_1} + i\gamma_c/2)\tau'} \mathcal{E}_{S_1}(\tau') \mathcal{E}_L^*(\tau') \right], \tag{7d}$$

where $\tau = t - z/c$ is the retarded time, and $v_a = c$ and $n_a = 1$ on the left-hand sides and the right-hand sides of Eqs. (3) respectively. of the integral terms in Eqs. (7a) and (7b) are evaluated approximately by making an adiabatic assumption (see below) about the fields, then the equations for $\mathcal{E}_{S_1}$ and $\mathcal{E}_{A_1}^*$ collinear along z are equivalent to Eq. (4) of BS,[1] and can be solved analytically if $\mathcal{E}_L$ is assumed constant.

III. NUMERICAL METHODS AND DISCUSSION

The dependence of the fields in Eqs. (7) on the spatial variables have been suppressed to simplify notation and emphasize their dependence on the retarded time. If the x derivatives are dropped, $\mathcal{E}_L$ is treated as a constant, and the τ' integrals are evaluated in the adiabatic-following approximation (i.e., treat the fields in the integrands as constant at $\tau' = \tau$, evaluate the resulting integrals, and drop all transient terms), then the steady-state equations of BS (Ref. 1) follow. As a check on the correctness of the numerical procedures used to solve Eqs. (7), the collisional damping was taken to be very large (for zero detunings δ_a) and the equations were solved for retarded times sufficiently long to produce agreement with the steady-state analytic solution of the BS (Ref. 1) equations. These numerical procedures consist of the use of the trapezoidal rule to evaluate the τ' integrals and (dropping the x derivatives in a one spatial derivative approximation) the integration of the resulting set of coupled differential equation along z from 0 to 300 cm using an efficient, internally-chosen variable step size, extrapolation method.[13] This procedure is checked internally by use of an explicit, two-point central-difference algorithm to integrate along a limited range in z (0–10 cm) and the extrapolation algorithm to evaluate the τ' integrals (this procedure producing a set of coupled integral equations).

In the former procedure, up to 101 equally spaced points in the τ grid for the interval $0 \le \tau \le 0.2$ ns had to be chosen to ensure the calculation of smooth pulses along z. This produces a set of 101 coupled differential equations, for each field, requiring integration along z. An internal check is the calculation of the total photon fluence [photons per cm^2 or the sum of squared moduli of the fields times $c/(8\pi\hbar\omega_a)$ integrated over τ] and its conservation along z. This fluence was conserved to high accuracy along the entire path. The input pulses in all cases are Gaussians with maxima at 0.1 ns and a τ scale parameter equal to 25 ns^{-1}. The peak input intensity is 1 GW cm^{-2} for the laser and 9% of this for the first Stokes.

The one-dimensional (i.e., collinear) version of the theory described above is used to study the convergence of a higher-order Stokes and anti-Stokes contributions to SRS. Figure 2 shows efficiencies (fraction of the total photon fluence for each pulse) for a second-order calculation. The second-order anti-Stokes pulse is too small to be on scale. Note the smallness and oscillatory character of the first-order anti-Stokes and second-order Stokes pulses. The one-dimensional theory is also used to study the effect of phase matching on anti-Stokes pulse generation in a first-order calculation (Fig. 3). The x derivatives in Eqs. (7) are dropped, but nevertheless the angles θ_{S_1} and θ_{A_1} (Fig. 1) are chosen to make $\Delta k_x \simeq \Delta k_z \simeq 0$ [Eqs. (2)]. These choices are 1.95×10^{-3} and 1.66×10^{-3} radians respectively, and the magnitude and character of the first-order anti-Stokes pulses are very different from the collinear case. The anti-Stokes pulse is now smooth and

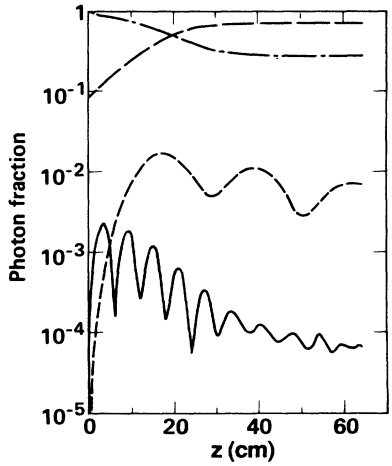

FIG. 2. Convergence of a collinear calculation (efficiency vs z). The gas pressure is 1 atm, the peak laser intensity 1 GW cm^{-2}, and the peak seed Stokes intensity 0.09 GW cm^{-1}. Long-short dashed line, laser; long dashed line, first Stokes; short dashed line, second Stokes; solid line, first anti-Stokes.

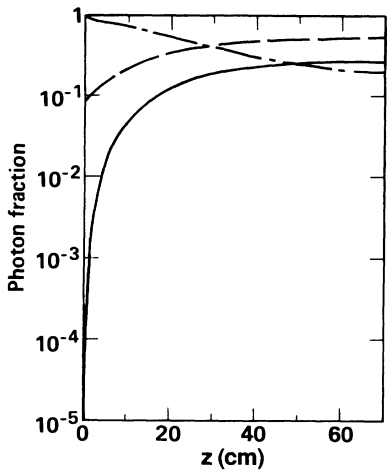

FIG. 3. Collinear calculation for phase-matched conditions (efficiency vs z). The other conditions are the same as in Fig. 2.

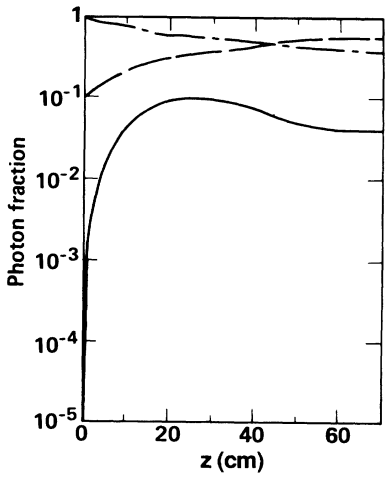

FIG. 5. Two-dimensional calculation for phase-matched conditions (efficiency vs x for $z=52.5$ cm). The other conditions are the same as in Fig. 2.

has risen to an efficiency of more than 25%. However, the terms containing the x derivatives in Eqs. (7) are not small, and two-dimensional calculations for the first-order waves only were performed (Figs. 4, 5, and 6). The x derivatives were replaced by two-point central difference formulas for a uniform x grid of 16 points in the interval $-0.15 \leq x \leq 0.15$. Thus the equations are propagated along z on a rectangular grid of 101 τ and 16 x points. A finer x grid would be desirable but requires storage in the z integrator[13] which is quite large.

Figure 4 shows efficiencies versus x for $z=52.5$ cm. The laser and seed Stokes pulses are assumed initially to have rectangular peak intensities of 1 and 0.09 GW cm^{-2}, respectively, from $-0.05 < x < 0.05$ cm. The entire interval is taken to be much larger than the initial input interval in order to study Stokes and anti-Stokes pulse behavior in regions of x and z in which the forward-going laser pulse does not exist. Thus the well-developed peak at about 0.1 cm in the Stokes pulse represents "walk away" along positive x at about the point predictable from the direction of $\mathbf{k}_S$ in Fig. 1 (for $\theta_{S_1} \simeq 1.95 \times 10^{-3}$ rad). The anti-Stokes pulse oscillates along x, and, except for larger positive x, shows an expected out-of-phase character with the oscillating Stokes pulse. The overall effect of the oscillatory structure in the anti-Stokes pulse is to reduce the overall efficiency along z, summed over all x contributions (Fig. 5), such that the maximum anti-Stokes efficiency is reduced to less than 10%.

Figure 6 shows an example of the pulses versus τ for $x=0.01$ and $z=52.5$ cm, the point of maximum anti-Stokes production (Fig. 4). Note the well-developed "hole burning" in both the Stokes and laser pulses. Despite the development of complicated temporal-spatial structure, to-

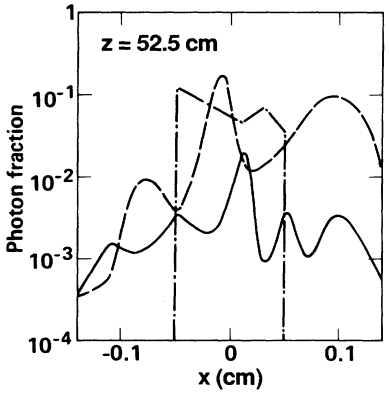

FIG. 4. Two-dimensional calculation for phase-matched conditions (efficiency vs z). The other conditions are the same as in Fig. 2.

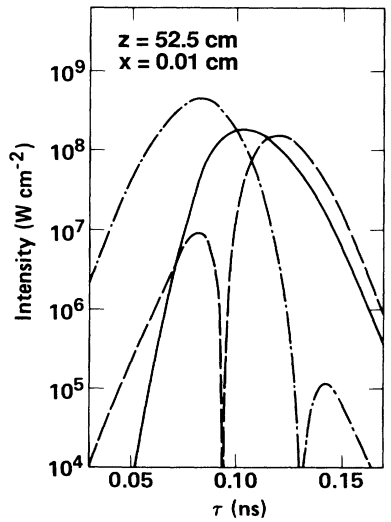

FIG. 6. Two-dimensional calculation for phase-matched conditions (intensity vs τ for $x=0.01$ cm and 52.5 cm). The other conditions are the same as in Fig. 2.

tal fluence is conserved in xz space to a high accuracy. This conservation and the correct reduction to the steady-state limit[1] contribute to our confidence in the numerical accuracy of the results.

IV. CONCLUSION

Stimulated Raman scattering in H_2 has been studied for collinear and slightly noncollinear geometries. Anti-Stokes Raman generation is effectively suppressed by dispersion-produced phase mismatch in the collinear case. Small angles of the Stokes and anti-Stokes waves can be found which produce phase matching in a first-order theory, and up to 25% anti-Stokes conversion efficiency is calculated. This high efficiency is reduced to less than 10%, however, when a theory having two spatial dimensions is used. Future theoretical work should include a further refinement of the transverse-dimension grid of numerical points, further modeling of the transverse intensity profiles based on experimental knowledge, and a theory which lets the direction of the anti-Stokes wave vector be arbitrary such that an angular distribution of anti-Stokes radiation can be calculated.

ACKNOWLEDGMENTS

The author would like to thank Merle Riley for cogent suggestions and advice during the course of this work. He would also like to thank Peet Hickman for communicating results corresponding to those of Fig. 2 from an independent numerical algorithm. This work is supported by the Naval Surface Weapons Center and the Strategic Defense Initiative Office. Partial support by Battelle Columbus Laboratories under Contract No. DAA629-81-D-0100 is also acknowledged.

---

*Permanent address: Lawrence Livermore National Laboratory, Livermore, CA 94550.

[1]N. Bloembergen and Y. R. Shen, Phys. Rev. Lett. **12**, 504 (1964).

[2]Y. R. Shen and N. Bloembergen, Phys. Rev. **137**, A1787 (1965).

[3]C. S. Wang, Phys. Rev. **182**, 482 (1968).

[4]R. L. Carman, F. Shimizu, C. S. Wang, and N. Bloembergen, Phys. Rev. A **2**, 60 (1970).

[5]V. Wilke and W. Schmidt, Appl. Phys. **16**, 151 (1978); **18**, 177 (1979).

[6]D. J. Brink and D. Proch, Opt. Lett. **7**, 494 (1982).

[7]J. A. Paisner and H. S. Hargrove, *Digest of Topical Meeting Excimer Lasers* (Optical Society of America, Washington, D. C., 1979).

[8]A. P. Hickman, J. A. Paisner, and W. K. Bischel, Phys. Rev. A **33**, 1788 (1986).

[9]A. L. Ford, Ph. D. thesis, University of Texas, Austing, 1972.

[10]Experimentally only the direction of the Stokes beam relative to the laser beam can be fixed, since the anti-Stokes light will have a spatial distribution which in principle includes all directions. However, we assume a fixed direction of the anti-Stokes light as that which, in conjunction with the direction of the Stokes beam, results in phase matching, i.e., $\Delta k \simeq 0$.

[11]A. Icsevgi and W. E. Lamb, Phys. Rev. **185**, 517 (1969).

[12]W. K. Bischel and M. J. Dyer, Phys. Rev. A **33**, 3113 (1986).

[13]R. Burlirsch and J. Stoer, Numerische Mathematik **8**, 1 (1966).